USGS HIGH-RESOLUTION TOPOMAPPING OF MARS WITH MARS ORBITER CAMERA NARROW-ANGLE IMAGES

Randolph L. Kirk*, Laurence A. Soderblom, Elpitha Howington-Kraus, and Brent Archinal
Astrogeology Team, U.S. Geological Survey, Flagstaff, Arizona (rkirk@usgs.gov)

Commission IV, Working Group IV/9

KEY WORDS: Mars, topographic mapping, photogrammetry, photoclinometry, softcopy, extraterrestrial mapping

ABSTRACT

We describe our initial experiences producing controlled digital elevation models (DEMs) of Mars with horizontal resolutions of ≤10 m and vertical precisions of ≤2 m. Such models are of intense interest at all phases of Mars exploration and scientific investigation, from the selection of safe landing sites to the quantitative analysis of the morphologic record of surface processes. Topomapping with a resolution adequate to address many of these issues has only become possible with the success of the Mars Global Surveyor (MGS) mission. The Mars Orbiter Laser Altimeter (MOLA) on MGS mapped the planet globally with absolute accuracies <10 m vertically and ~100 m horizontally but relatively sparse sampling (300 m along track, with gaps of >1 km between tracks common at low latitudes). We rely on the MOLA data as the best available source of control and process images from the narrow-angle Mars Orbiter Camera (MOC-NA) with stereo and photoclinometric (shape-from-shading) techniques to produce DEMs with significantly better horizontal resolution. The techniques described here enable mapping not only with MOC but also with the high-resolution cameras (Mars Express HRSC, Mars Reconnaissance Orbiter HiRISE) that will orbit Mars in the next several years.

1. Introduction

Accurate topographic information, and, in particular, high-resolution digital elevation models (DEMs) are of intense interest at all phases of Mars exploration and scientific investigation, from landing site selection to the quantitative analysis of the morphologic record of surface processes. Unfortunately, the availability of extremely high resolution topographic data has hitherto been limited. The current "gold standard" for martian topographic data, the Mars Orbiter Laser Altimeter (MOLA; Zuber et al., 1992; Smith et al., 1999; 2001) has collected data globally with astonishingly high accuracy, but the resolution of this dataset is only about 300 m along track and, in many places near the equator, adjacent MOLA ground tracks are separated by gaps of one to several kilometers. Viking Orbiter images provide stereo coverage of the entire planet at low resolution and expected vertical precision (EP, a function of image resolution and stereo viewing geometry) but highest resolution stereo coverage only of limited areas (Kirk et al., 1999b). Given that the minimum separation of independent stereo measurements is about 3 pixels because of the necessity of matching finite-sized image patches, the highest resolution Viking images, at about 8 m/pixel, support stereomapping only at horizontal resolutions >24 m. Photoclinometry, or shape-from-shading (Kirk, 1987) can be used to produce DEMs at the pixel resolution from single images but the results depend on the accuracy of atmospheric and surface radiative transfer models (Kirk et al., 2000b, 2001). Calibration of photoclinometry against MOLA data (Herkenhoff, et al., 1999; 2002; Soderblom et al., 2002) or against stereo DEM data as reported here promises to reduce uncertainties about the inferred scale of relief, but albedo variations can still lead to artifacts in the resulting DEMs.

The MOC-NA camera, with a maximum resolution of 1.5 m/pixel (Malin et al., 1992; 1998; Malin and Edgett, 2001), offers the prospect of stereotopographic mapping at a horizontal resolution of ~5 m and EP ~ 1 m. MOC-NA stereo coverage is limited because most images are obtained with nadir pointing and are not targeted to overlap one another, but at least several tens of MOC-MOC stereopairs do exist. In addition, because of the urgent need to assess the safety and trafficability of candidate landing sites for the Mars Exploration Rover (MER) mission, further imaging, including stereo, of these sites is an important objective of the MGS extended mission. It is also likely that some MOC images will provide useful stereo coverage when paired with oblique Viking Orbiter images. A capability for stereomapping with the MOC-NA images is therefore highly desirable, but the pushbroom scanner geometry of the camera means that new software is required, as that developed for framing cameras, like those of the Viking Orbiter, will not suffice. The other main challenges in working with MOC-NA data are identifying suitable stereopairs and providing adequate geodetic control for such high-resolution images. In this paper we describe our methods and results for the Mars Pathfinder and candidate MER landing sites, expanding on a pair recent abstracts (Kirk et al., 2001b; 2002) that focused respectively on the methods and on the MER sites. We are not the only group working in this area; results of stereomatching uncontrolled MOC images are reported in a recent abstract by Ivanov and Lorre (2002)

2. Methodology

2.1 Software Implementation

The software packages, specialized hardware, and workflow for the MOC mapping reported here are the same as those we use

* Correspondence author.

for stereoanalysis of a wide range of planetary datasets (Kirk et al., 1999a; 2000a; Rosiek et al., 2001a; 2001b; Howington-Kraus et al., 2002a; 2002b). We use the USGS in-house digital cartographic software ISIS (Eliason, 1997; Gaddis et al., 1997; Torson and Becker, 1997) for mission-specific data ingestion and calibration steps, as well as "two-dimensional" processing such as map-projection and image mosaicking. Our commercial digital photogrammetric workstation, an LH Systems DPW-790 running SOCET SET software (© BAE Systems; Miller and Walker, 1993; 1995) includes special hardware for stereo display of images and graphics, and is used mainly for such "three-dimensional" processing steps as automatic and manual measurement of image tiepoints; bundle-block adjustment of image orientations to conform to geodetic control; and automatic extraction and manual editing of DEMs. The ability to view DEM data as graphics overlaid on the images in stereo in order to detect and interactively edit errors is the single most important reason for using the commercial system.

In order to work with planetary data, we have written a set of translator programs drawing on both ISIS and the SOCET SET Developer's Toolkit (DEVKIT) to import images and geometric metadata from ISIS into SOCET SET and export DEMs and orthoimage maps back to ISIS. Images from planetary framing cameras (e.g., Viking, Clementine) can then be analyzed with the framing camera sensor model software supplied as a basic part of SOCET SET. (A sensor model consists of software that carries out the transformation between image and ground coordinates and vice versa, plus a variety of housekeeping routines.) The DEVKIT lets us implement and install sensor models for other instruments, such as the Magellan synthetic aperture radar (Howington-Kraus et al., 2002a). After beginning a similar in-house development of a sensor model for the MOC camera, we were able to take a substantial "shortcut" by making use of the generic pushbroom scanner model included in SOCET SET and writing only the software needed to import MOC images and set them up for use with this model.

The generic scanner model computes a physically realistic description of the process by which a scanner image is built up. It is "generic" in the sense that the following parameters must be specified and can be different for different cameras and/or images from the same camera:

- Image size; relation between line number and time
- Camera focal length and lens distortion polynomial
- Camera trajectory in the form of position and velocity at a series of equally spaced times spanning acquisition of the image, to be interpolated
- Camera orientation relative to the vertical and flight direction (nominally assumed constant)
- Corrections to the trajectory and orientation, normally initialized as zero and estimated as part of the bundle-adjustment process
  - Position and velocity offsets in the along-track, across-track, and vertical directions
  - Angular offsets around three orthogonal axes, angular velocities, and angular accelerations

These parameters suffice to describe not only the MOC-NA but also the wide-angle (WA) cameras, which have been used to obtain global stereo coverage with 240-m resolution (Caplinger and Malin, 2001); the infrared scanner of the THEMIS instrument on the Mars Odyssey Orbiter (Christensen et al., 1999) the Mars Express High Resolution Stereo Camera (HRSC) with multiple detector lines for single-pass stereo imaging at 10 m/pixel (Albertz et al., 1992); and the HiRISE scanner selected by NASA for the 2005 Mars Reconnaissance Orbiter mission (McEwen et al., 2002). Not only can the generic scanner model be used with images from any of these cameras, SOCET SET permits bundle-adjustment and stereo DEM collection with any combination of scanner and framing camera data in a single project. To date, we have written software to collect the necessary information from both MOC-NA and WA image labels, convert geometric quantities from the inertial coordinate system used by ISIS to the local Cartesian system used by SOCET SET, and write this supporting data in the needed format.

The main limitation of the software that affects its use with MOC-NA images is the nominally constant orientation of the camera. Images obtained (during the aerobraking phase of the MGS mission) by rotating the spacecraft do not fit this model, and our experiments with representing the spacecraft rotation by using the adjustable parameters have so far been unsuccessful. An enhancement of the sensor model promised for a future release will allow an arbitrary time history of camera orientation to be specified. The limited set of adjustable parameters in the model also has its drawbacks, and this is unlikely to be changed. The low-order (smooth) position and pointing corrections possible with these parameters cannot address the high-frequency undulations of the MGS spacecraft that plague some MOC stereopairs as discussed below. Nor does the SOCET SET bundle-adjustment software understand that images from a multiline scanner such as HRSC come from the same spacecraft and are subject to the same position and pointing corrections as a function of time. To address these shortcomings it is necessary to implement more capable bundle-adjustment software outside SOCET SET and then import the corrected geometric data derived with such software. We have proposed to NASA to add pushbroom scanner capability to the RAND bundle-adjustment software recently taken over by the USGS. We plan initially to model single-line scanners, including high-frequency pointing oscillations. Modeling of multiline scanners could be undertaken at a later date if adequate orientation data and/or adjustment software to produce such data are not produced within the Mars Express mission.

2.2. Identification of Stereoimagery

Identifying suitable pairs of MOC-NA images for stereoanalysis is a significant challenge, given that more than 30,000 images have been released to date but the typical image covers only about one one-millionth of Mars's surface area. We have pursued several approaches to identifying pairs for initial testing of our software. First, MOC press releases on the Malin Space Science Systems (MSSS) website http://www.msss.com/mars_images/moc/MENUS/moc_by_date.html include a number of anaglyphs made from NA stereopairs. Unfortunately, the most dramatic of these stereo views are also the most recent (press releases MOC2-256, 282, 283, and 287) and contain images not yet released. Earlier releases (Table 1) show the Viking 1 (MOC2-44), Mars Polar Lander (MOC2-255), and Mars Pathfinder (MOC2-46; Figure 1) landing sites. Of these, the last was selected for initial testing because we have previously mapped parts of the region with both Viking Orbiter (Howington-Kraus et al., 1995) and Mars Pathfinder IMP (Kirk et al., 1999a) images. The stereo pair unfortunately does not cover the actual landing point, but does include "Big Crater" (prominent in the lander images) and plains to the south and west. Non-stereo MOC coverage of the landing point shows that it and the plains south of Big Crater are extremely similar in texture and morphology.

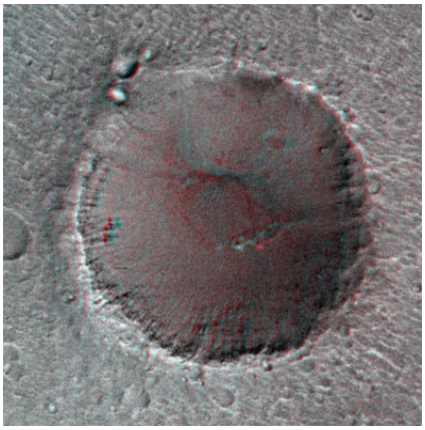

Figure 1. Anaglyph of "Big Crater" (1.5 km in diameter, located 2.2 km SSE of Mars Pathfinder landing point), taken from MSSS press release MOC2-46. Figure shows a small part of stereo overlap of images and SP1-23703SP1-25603, which extends to Sand W (Fig. 2) but unfortunately does not cover Pathfinder site. For correct stereo impression, view with red filter on right eye.

The optimal way to identify stereopairs is obviously through an exhaustive, automated search of catalog data. We previously conducted such a search for the ~45,000 Viking Orbiter images, which yielded ~360,000 potential pairs (i.e., each image overlaps about 8 others), only a fraction of which had useful EP (Kirk et al., 1999b). Here, we report on similar searches of the MOC-NA catalog (the cumindex.tab file on the official MOC releases, plus similar data for pre-released, extended-mission images of the MER landing sites). An initial search of catalog data, carried out in August 2001, generated 4,872 candidate pairs from the list of 31,901 images through mission phase E06. This list was narrowed by excluding those with stereo convergence angles too large or too small, and those with dissimilar illumination (criteria similar to those used by Kirk et al. (1999b) and adopted from the work of Cook et al. (1996)). This step yielded 158 candidate pairs, 18 of which were located in regions under consideration as MER landing sites; because of the urgency of assessing the safety of these sites, we limited further consideration to the images there. We interactively examined these images and eliminated the ones with little or no overlap, and those with low image contrast due to atmospheric opacity. The image pairs found for each of 4 sites are included in Table 2. Results of mapping and roughness analysis for these image sets (plus the Pathfinder site) were reported in a recent abstract (Kirk et al., 2002).

Unfortunately, a more recent search of the MOC catalog through mission phase E13 produced many new candidates but only a few additional usable pairs, all of which had already been found by interactive search as described below. The low success of this search may be due in part to a MOC targeting strategy that minimizes stereo overlap with past images in order to maximize new area covered, and in part to the substantial errors (comparable to or greater than the image width) in the image footprint locations catalogued on the basis of predicted spacecraft ephimerides. An additional source of error is the approximate nature of the criteria we used for automatically determining intersection of images: a test was made whether any of the corners of the minimum bounding rectangle (MBR) of one image in latitude and longitude fell inside the MBR of the other image. We plan in the near future to repeat the search for MOC image pairs, incorporating a rigorous test for the overlap of the actual image footprints (not their MBRs) and calculating footprints calculated from the mission ephemerides (rather than using those from the cumulative index) to reduce positional errors. Because coordinate errors cannot be eliminated entirely, this search will probably still require a final, manual step of checking the images for their actual overlap and contrast, and it may be useful to "pad" the image footprints by an amount corresponding to the coordinate errors in order to search for images that overlap in fact but not according to their SPICE data. We will also look for mixed pairs of MOC and Viking images that yield usable stereo.

Maps of MOC-NA image coverage of prospective MER landing sites (http://marsoweb.nas.nasa.gov/landingsites/mer2003/mer2003.html) provide another resource for locating stereopairs in these areas of highest current interest. Note that the interactive maps on this site do not always contain the most recent releases, but the site contains links to thumbnails of these images and context images for them that are also useful. Image footprints have been placed interactively in these maps and context images, so they are more accurate than the catalog information but not error-free. Pairs of images whose footprints appear to overlap must be screened to determine if they actually overlap, if they have useful stereo geometry (at a minimum, at least one off-nadir image), and if the illumination is consistent enough between images to permit automatic stereomatching. Additional image sets were subsequently rejected for a variety of reasons including inadequate overlap, obscuration of the surface by atmospheric dust, changes in surface appearance between the two images due to wind activity, missing spacecraft orientation data, and, in one case, an imaging strategy not supported by our software. Oblique image AB1-07704, which crosses nadir images M08-01457 and M09-01839 in the Hematite area, was obtained with the spacecraft rotating, and our attempts to model this image with the current software have been unsuccessful. In total, we have identified 16 usable stereosets within the MER landing sites and extracted DEMs from 10, including at least one at each of the six sites except Hematite (Table 2). It is noteworthy that all of these images were obtained by 2x2 or 4x4 summation of pixels, so that their resolutions are not as high as the MOC-NA camera is capable of. In all cases, however, the resolutions are better than the best Viking Orbiter images.

2.3 Geodetic Control

Our experience with map-projecting and comparing MOC-NA and WA images indicates that errors of position (combining both spacecraft position and pointing errors) are often <100 m but occasionally greater, especially for off-nadir images. This is adequate to produce uncontrolled mosaics of WA images (≥240 m/pixel resolution) but inadequate for the higher resolution NA data. In particular, 100-m relative horizontal errors between images of a stereopair will give rise to comparable vertical errors in the DEM. It is therefore highly desirable to use a bundle-adjustment process to bring the images into consistency with external control. This process is made challenging by the large gap in resolution between the NA images and the next-best datasets available for control. The MOLA dataset, with estimated absolute accuracies of <10 m vertically and ~100 m horizontally (Neumann et al., 2001), is the ultimate source of control, but the spacing of MOLA footprints is hundreds to thousands of MOC-NA pixels. Direct comparison of the MOC images with MOLA profiles or gridded MOLA data is therefore helpful in bringing the stereomodels into vertical correspondence with the altimetry but not very useful for improving their horizontal positioning. In our opinion, the best approach to refining the horizontal position of MOC-NA images and stereomodels would be to tie other images of intermediate resolution to the MOLA data and then

tie the MOC images to these. At the moment, this necessarily means Viking Orbiter images—the best available resolution at each of the MER sites is indicated in Table 2—but over the next few years the visible light camera of THEMIS will provide 18 m/pixel CCD frame images of much of Mars. We routinely use intermediate resolution frames to transfer control from MOLA in our stereomapping with Viking images (Rosiek et al., 2001a) but we have yet to test the process with MOC data. The use of a large number of ties between intermediate-resolution images and MOC-NA will be essential to modeling and correcting the high-frequency oscillations of the MGS spacecraft with the advanced bundle-adjustment software we hope to develop. As discussed above, the bundle-adjustment capability currently available as part of SOCET SET does not include modeling of such high-frequency oscillations.

For the purposes of landing site selection (as opposed to precision landing), precise relative topographic data (from which slope estimates can be made) is more important than absolute accuracy. Our efforts to control the images listed in Tables 1-2 have therefore focused on bringing the stereomodels into vertical agreement with MOLA data and not on improving horizontal positioning. For each stereopair, we select a well-distributed set of points (typically 10–20) whose locations can be measured on both MOC images. We then assign each point the elevation interpolated from MOLA data at its *a priori* horizontal location. These heights are used as constraints in the bundle-adjustment process, but no constraints are placed on horizontal positions. The form of the MOLA data used in our control process is an in-house USGS product, gridded at 500-m ground sample distance and adjusted to conform to the most recent set of Mars cartographic constants recommended by the International Astronomical Union and International Association of Geodesy (Duxbury et al., 2002; Seidelmann et al., 2002). Similar products for the candidate MER landing sites are available online at http://webgis.wr.usgs.gov/mer/.

The control process for the stereopair near the Mars Pathfinder landing site was even simpler. Rather than determining an interpolated MOLA elevation for every tiepoint, we estimated the average MOLA elevation for the region of the stereomodel and loosely constrained a subset of tiepoints (away from Big Crater and other obvious relief) to have this elevation. The result is to underestimate any net regional slope of the stereomodel.

Our attempts to control the stereopairs listed in Table 2 have been complicated by transmission errors in one or both of the images. It is a characteristic of the Huffman coding used to compress these high-resolution images that signal degradation between the spacecraft and ground station can cause the loss of blocks of image lines; if the degradation is extensive, it may not be known how many lines were lost. When this happens, the correct acquisition times of the lines after the gap (needed in sensor model calculations) are lost. We are working on semiautomated approaches to reconstructing the image line count from information returned in the images, but for the time being our approach to working with MOC data after a data dropout is strictly empirical. We first compare the corrupted image with an uncorrupted image of the same region, estimate the number of missing lines, and insert this number of blank lines into the gap to approximately restore the image. We then control the image, being careful to place pass-points only in the section below the gap (if the section above the gap is needed for mapping, we treat it as an independent image) and allowing a larger than usual along-track adjustment of the spacecraft position to account for the error in reconstructing the gap size.

The final complication to the control process, encountered for most MER landing site stereopairs (but not for the Pathfinder site), arises from the high-frequency spacecraft pointing errors or "jitter" alluded to previously. Pointing oscillations in direction of the stereobase (i.e., across-track for most MOC pairs) mimic elevation-related parallax and result in artifacts in the DEMs in the form of "stripes" elongated across-track; these are also reported by other users of MOC stereoimagery (Ivanov and Lorre, 2002). From the dimensions of these DEM stripes we can infer the magnitude (highly variable but as much as 50 μRad or more than 10 MOC pixels) and frequency (0.1–1 Hz) of the oscillations that cause them. Oscillations of similar amplitude are seen in the spacecraft pointing data but the 2 second sampling interval of this dataset results in the jitter being aliased to much lower frequencies. Jitter in the direction orthogonal to the stereobase (normally, along-track) results in localized mismatches between the images that confound both automatic and interactive DEM extraction. It is important to note that the likely magnitude of high-frequency pointing errors was known to MGS engineers (if not to users of the data) even before the mission. The MGS spacecraft was not specifically designed for high resolution stereoimaging, and the MOC camera must share the platform with other instruments and articulated solar panels and high gain antenna, all of which are sources of high-frequency vibration at a magnitude that does not impact the primary MOC goal of imaging for geologic interpretation.

The rigorous and therefore desired approach to correcting for these spacecraft pointing oscillations is to collect a dense set of tiepoints between the MOC stereoimages, intermediate-resolution frame images, and the MOLA DEM, and to perform a bundle-adjustment with specialized software that includes an appropriate parameterization of the high-frequency motion. Until such software can be developed, we have been forced to develop alternative procedures to work around the problem. If the DEM can be collected, ad hoc processing to suppress the stripes in the direction of the parallax base is relatively straightforward. We first take the difference between the stereo-derived and MOLA DEMs at matching resolution, then apply a series of digital filters (lowpass across the image strip, highpass in the flight direction) to get an estimate of the pointing-related artifacts that can then be subtracted from the stereo DEM. Of course, this procedure also suppresses real topography if it consists of features (e.g., ridgelines) that happen to cross all or most of the image. The narrower the region of stereo overlap, the more difficult it becomes to make a useful distinction between artifacts and real topography.

For stereopairs with the most severe jitter, it may be impossible to collect a DEM based on a single control solution with the existing software: if corresponding image lines are registered in one part of the pair, they may be so misaligned elsewhere that automatic stereomatching fails and the brain is incapable of fusing them in stereo. In such cases we have found it necessary to break the images into smaller sections and adjust the across-base orientation angle separately for each section. Sectional DEMs can then be collected, edited as usual, and merged. The resulting product is necessarily imperfect, as a continuous oscillation of the across-base angle has been corrected in a piecewise fashion, but the discontinuities in the DEM that result can be minimized. Needless to say, this process is undesirable both because it is extremely time-consuming and because it is approximate and necessarily subjective.

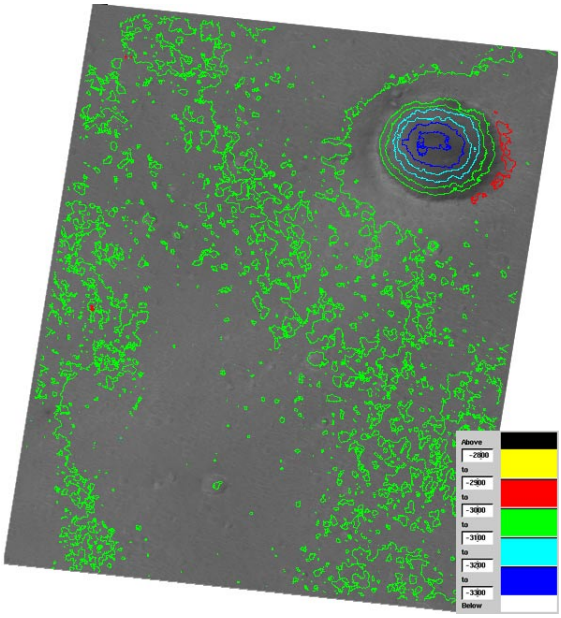

Figure 2. Orthorectified MOC image SP1-23703 with stereo derived contours (contour interval 50 m, color interval 100 m). Total relief from floor to rim of Big Crater is 300 m. Automatic stereomatching was successful except for a single artifact (red dot at center left).

2.4 Analysis of DEM Data

We describe the process of DEM analysis in some detail for the Pathfinder site, which was the first MOC stereopair mapped and for which there are a variety of datasets available for comparison. Figure 2 shows image SP1-23703, orthorectified, with superimposed contours derived from the stereo DEM. The low relief of this region is readily apparent: from the bottom to the top of Big Crater the total relief is 300 m. The most prominent feature in the unedited DEM, apart from the crater, is an apparent peak ~75 m high and 120 m across the base, located near the middle right of the image. This is not a real topographic feature, but an artifact caused by local failure of the automatic matching algorithm. It is also visible in a perspective view of the DEM (Figure 3). The high overall success of the SOCET SET matcher is gratifying, given the relatively low contrast of the images.

Figure 4 shows the image and DEM data for a portion of the stereomodel excluding both Big Crater and the matching artifact. This section was selected for statistical analysis to characterize the flat part of the landing site. The DEM in this area is consistent with our description based on IMP data of the landing site topography as dominated by ridges and troughs

Figure 3. Perspective view of Big Crater from the northwest. 3 m/pixel MOC image SP1-23703 has been draped over 10 m/post stereo-derived DEM. Vertical exaggeration is 2. Matching artifact is visible as a small "hill" in the background. Colors are arbitrary, intended only to suggest the appearance of the martian surface.

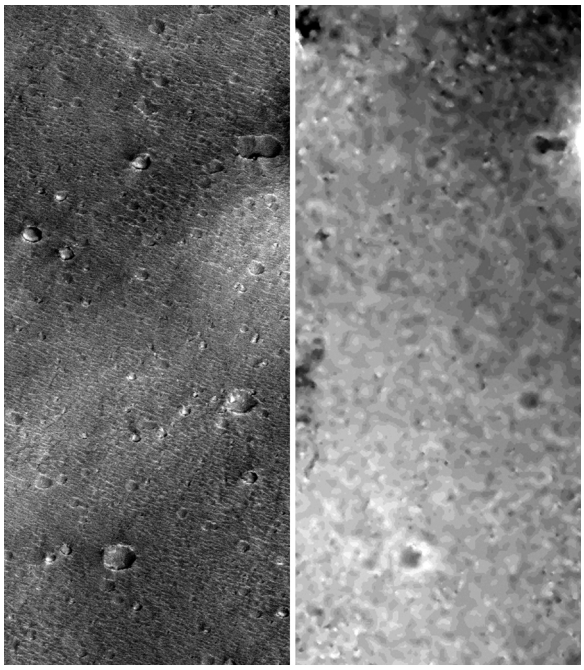

Figure 4. Orthoimage and DEM data (shown at right as grayscale) for ~2.6 x 7.5 km section of the MOC stereomodel SP1-23703/SP1-25603 to the W and S of Big Crater. This region was selected for slope analyses and comparison with results from the Mars Pathfinder lander, which is located on similar plains to the N. Total range of elevations in this area is ≤5 m.

with a typical amplitude of a few meters and a wavelength of several tens of meters (Kirk et al., 1999a). The smallest ridges are not fully resolved in the DEM but a pattern of somewhat larger ridges can be seen. Comparison of the image and DEM tends to support our previous assertion that many of the bright albedo features in the images are associated with local topographic highs. These are probably strips of light-colored, rock-free sediment similar to those seen (also along ridges) near the lander and interpreted as dunes by Greeley et al. (2000).

Figure 5 shows the distribution of bidirectional slopes derived from the DEM area in Fig. 4, for a north-south baseline of one post (approximately 12 m). The root-mean-squared (RMS) slope is 4.2° but, as the histogram shows, the slope distribution has longer tails (i.e., extreme slopes are relatively more common) than for a Gaussian distribution. Slopes on this baseline are in the range ±14.1° for 99% of the test area. For the adirectional slope (maximum slope in any direction, or gradient) over the same baseline, the 99th % ile is 15.8°.

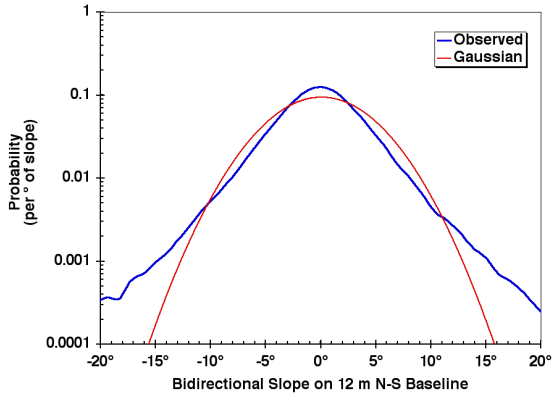

Figure 5. Histogram of bidirectional slopes over a 1-post (12 m) N-S baseline from the portion of the MOC DEM near Big Crater seen in Fig. 4. Gaussian distribution with the same RMS slope (4.2°) as observed is shown for comparison. Large slopes are significantly more common than the Gaussian model would suggest.

It is also of interest to look at the RMS slopes over a variety of distance scales. Not only do slopes over long baselines and local slopes have different implications for landing safety and rover trafficability, but this type of analysis lets us compare the MOC DEM with other topographic datasets for the region. If $z(x)$ is a profile of height as a function of horizontal coordinate, and Δ is a horizontal baseline ("lag"), then the one-dimensional autocovariance function $\rho(\Delta)$ is given by

$$\rho(\Delta) = \langle z(x)\, z(x+\Delta) \rangle$$

where the brackets $\langle\ \rangle$ indicate an ensemble average over both x and multiple parallel profiles. From the above definition, it is easy to show that the RMS (dimensionless) slope over the baseline Δ is given by

$$\Theta_{RMS}(\Delta) = \sqrt{\{\, 2\,(\rho(0) - \rho(\Delta)) / \Delta \}}.$$

Figure 6 is a plot of $\Theta_{RMS}(\Delta)$ calculated from autocovariance estimates obtained by fast Fourier transform techniques for four independent DEMs covering different parts of the Mars Pathfinder landing ellipse at a variety of scales. Dimensionless slopes have been multiplied by the conversion factor from radians to degrees, so the larger slope angles are slightly overstated here. Each of the curves shows a characteristic "dogleg" shape, with a steep section with $\Theta_{RMS}(\Delta) \propto \Delta^{-1}$ for large Δ and a shallower log-log slope at small Δ (the highest resolution dataset does not show an extended steep section but the beginning of a rolloff is nonetheless visible). The steep curves at baselines that are large relative to the respective DEM reflect the fact that each of these topographic models has been controlled essentially to be level overall, so slopes on the longest baselines are underestimated. The "dogleg" in each curve thus reflects the resolution at (and below) which relative topography and slopes are unaffected by errors in control. This scale is especially small (in relation to the DEM size) for our MOC stereomodel because we controlled it to a constant elevation rather than to MOLA data. The continuity of the shallow portions of the Viking photoclinometry, MOC stereo, and IMP stereo curves is striking, given that no two of these datasets cover precisely the same area. The photoclinometry data are taken from Viking image 004A72, which contains only smooth plains similar to those near the lander and south of Big Crater. In contrast, the Viking stereo data cover almost the entire 100x200-km Pathfinder landing ellipse, which contains more rugged features such as craters and streamlined islands (Howington-Kraus et al., 1995). Photoclinometry on images from rougher parts of the landing ellipse yields slope estimates as much as a factor of two greater than for 004A72. The curve for IMP data is derived from a DEM extending 10 m on each side of the lander (Kirk et al., 1999a). Slope estimates over larger baselines can be computed from coarser IMP DEMs extending farther from the lander, but the RMS slope is systematically underestimated in these datasets because much of the distant landing site was hidden behind ridges and the DEMs therefore contain (unrealistically) smooth patches interpolated from actual data for the visible areas. We have therefore not included these estimates in Fig. 6, but their lower RMS slopes are consistent with the value of 4.7° at 1-m baselines quoted by Kirk et al. (1999a).

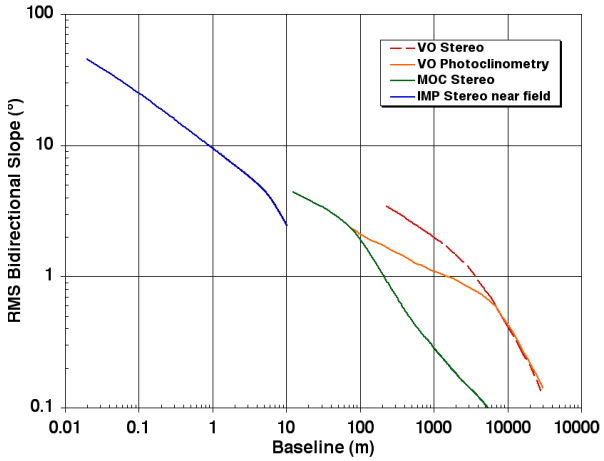

Figure 6. RMS slopes of regions near Mars Pathfinder landing site calculated as described in text from DEMs based on images of a variety of scales and sources. VO stereo DEM covers most of Pathfinder landing ellipse (including some high-relief features) and was interpolated from contours obtained by analytic photogrammetry of 38 m/pixel Viking images. VO photoclinometry DEM was obtained from 38 m/pixel image 004A72 of smoothest part of landing ellipse, highpass filtered to suppress artifacts of photoclinometry. MOC stereo DEM derivation is reported here. IMP stereo DEM covers the region from the lander to 10 m at GSD of 2 cm, and was interpolated from data collected on IMP stereopairs with highly variable ground spacing. Slopes over smaller baselines for each DEM are expected to be most accurate and are consistent between datasets. Slopes at longest baselines for each dataset are affected by the control process and systematically underestimate real slopes.

There is no necessary reason for the shape of the slope distribution to be independent of baseline, but it is likely that this assumption is at least approximately correct over modest baseline variations, and we have found in practice that slope distributions for many areas of Mars evaluated at various baselines almost always have the long-tailed, nearly exponential shape seen in Fig. 5. Because the distribution shape does not change greatly, the curves in Fig. 6 can also be used to scale estimates of percentile slopes measured at one baseline to a slightly different baseline. On this basis the 99th %ile adirectional slope for the MOC stereo DEM can be extrapolated to a baseline of 5 m, giving a value of 20.4°. Five meters is approximately the lengthscale at which the MER (and Pathfinder) airbag system "feels" the topography on which it lands, and consequently one criterion for a safe landing site is ≤1% probability of encountering a slope in excess of 15° over this baseline. By this criterion, the Pathfinder site was *not* safe, a fact that (in hindsight, fortunately) could not be ascertained prior to the 1997 landing.

The log-log slope of the curves in Fig. 6 can be interpreted in terms of fractal geometry (Turcotte, 1997): if $\Theta_{RMS}(\Delta) \propto \Delta^{H-1}$, where $0 \le H \le 1$ is the Hurst exponent, the fractal dimension of the surface is $D = 3 - H$. The Viking photoclinometry and MOC stereo datasets show a similar dimension $D \sim 2.3$, whereas for the IMP data $D \sim 2.4$. This difference may reflect the structural features (fluvial or eolian ridges vs. rocks) that dominate relief at different scales, but it should be borne in mind that the slope estimates are also affected by the noise properties of the data and method used to produce the DEM. In any case, we find it interesting that a straight-line extrapolation of the Viking photoclinometry curve from baselines ≥80 m yields slopes at centimeter scales that are within a factor of two of those measured *in situ*.

3. Application to Candidate MER Landing Sites

The 10 stereopairs from which we have collected DEMs of candidate MER landing sites are listed in Table 2. Analysis of the slope statistics for these sites was carried out as described above for the Pathfinder site. In addition, two-dimensional photoclinometry (Kirk, 1987) was used to generate DEMs of most of the sites at single-pixel (as opposed to three-pixel for stereo) post spacing. This technique, also known as shape-from-shading, amounts to the iterative, least squares adjustment of the DEM post elevations in order to make a shaded relief image calculated from the DEM fit the observed image. An important limitation of the method is that variations in surface reflectivity (albedo) are not generally accounted for in the shaded relief model. Areas of relatively constant albedo (at a minimum, more image contrast from topographic shading than from albedo variations) must therefore be selected for the results to be valid.

In order to obtain a quantitatively accurate DEM, it is necessary not only to have an accurate photometric model (i.e., bidirectional reflectance function) for the surface (Kirk et al., 2000b) but to account for light scattered in the atmosphere (Kirk et. al., 2001). Unless the degree to which image contrast is reduced by atmospheric scattering is correctly understood, the result will be a DEM with the correct qualitative shape but the wrong amplitude of relief, obviously useless for collecting slope statistics. A well-established approach to estimating the haze component of images for photoclinometry is to measure the brightness of a shadow and subtract this from the entire image. Unfortunately, the MOC orbit geometry precludes shadows in most images of the near-equatorial zone where the MER sites are located. We were able to use the shadow correction method for one nonstereo image (M07-01888, not in Table 2) of Athabasca Vallis. In the Hematite site, for which no stereo coverage and no shadows were available, we estimated the haze level by requiring that dunes there have the same relative contrast after haze correction as dunes (with the same incidence angle and azimuth relative to the Sun) in other images for which the haze was estimated as described below. Since the opposing slopes on dunes are controlled by relatively universal physical processes (Bagnold, 1954), they should be similar from place to place on Mars and provide a convenient reference for image contrast.

Alternative (and potentially more accurate) approaches to estimating the haze that should be subtracted from an image require a DEM from an independent source. For example, we have previously shown (Herkenhoff et al., 1999; Soderblom et al., 2002; Herkenhoff et al., 2002) that the haze level can be adjusted to bring the resulting photoclinometric DEM into agreement with a MOLA profile. Two important conditions for this method to work are, first, that the MOLA profile run close to the direction (i.e., up-sun) for which photoclinometric profiles are most accurate, and, second, that there be significant relief resolved by MOLA, which has a 300 m along-track sample spacing. The first condition is violated in the equatorial zone (illumination is roughly at right angles to the MOLA tracks) and the second is violated by many of the landing sites, which are deliberately chosen to be flat over large baselines. Use of a stereo-derived DEM circumvents both of these problems. We calculate a shaded-relief image from the stereo DEM by using a realistic surface photometric model but no atmospheric contribution. Provided the model resolves topographic features well enough that the shaded relief closely resembles the real image (this is readily evaluated visually so that a suitable subarea of the shaded relief model can be chosen

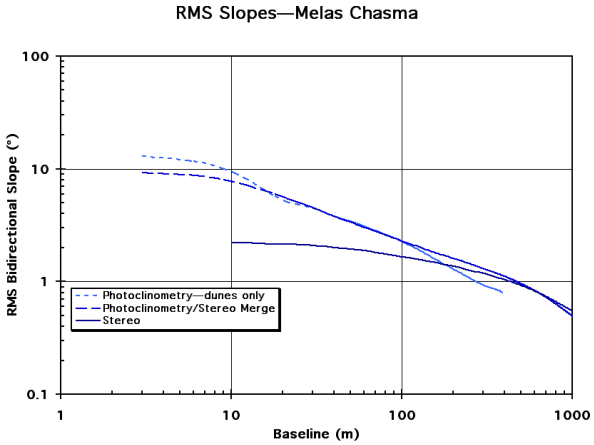

Figure 7. RMS slopes in a dune-covered region of Melas Chasma (stereomodel E02-00270/E05-01626) as a function of baseline; compare Fig. 6. Stereo DEM gives low slopes with little variation at baselines <100 m, suggesting that the site is extremely smooth, but photoclinometry reveals that dunes unresolved by the stereomatcher are much rougher. Figure also shows that stereo and photoclinometric DEMs can be merged to combine the absolute accuracy at long-baselines of the former with the high spatial resolution of the latter. (Curve for the merged DEM shows slightly lower slopes than for pure photoclinometry DEM at short baselines because it covers a larger area including some dune-free regions.)

for comparison), the intercept of a linear regression of image on shaded relief is the desired haze parameter.

With both stereo and photoclinometric DEMs available for most sites, it becomes important to determine which provides the most accurate slope estimates. The most important factor is the horizontal resolution of the two methods, which is readily addressed by Fourier analysis. Although the ~3-pixel post spacing of our stereo DEMs exceeds the 5-m baseline at which the slope must be estimated for the MER safety criterion, in most cases the slope-vs.-lag curve can be used to extrapolate the statistics to 5 m with results confirmed by photoclinometry. A notable exception occurs in Melas Chasma (Figure 7). The stereo DEM of this region is extremely smooth, but the photoclinometric results (and visual examination of the images) shows that the stereomatcher just misses resolving the small but very rugged dunes. Interactive spot measurements of the dune heights and slopes in stereo confirm the photoclinometric

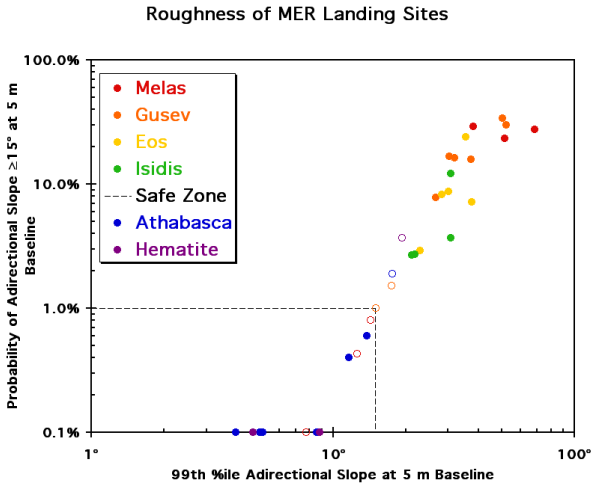

Figure 8. Summary of the roughness of regions of the 6 candidate MER landing sites, relative to the safety criterion of ≤1% probability of slopes in excess of 15° at the 5-m baseline sensed by the landing airbag system. Symbols for DEM areas that are unrepresentative or compromised by resolution effects or albedo variations are subdued.

results. Other conditions that affect the relative accuracy of the stereo and photoclinometric DEMs are albedo variations (as noted above, these will create artifacts in the photoclinometric DEM, making the surface appear rougher than it is) and sampling effects. Because two-dimensional photoclinometry is extremely computer intensive, it is limited to smaller areas that in some cases may not reflect the overall properties of a given site as well as a larger, stereo-derived DEM. In Figure 8, all slope estimates are shown but those deemed inappropriate because of resolution, albedo, or sampling effects are subdued. (The rationale for preferring certain subareas over others is given in Table 3, where the non-preferred values are grayed out and additional slope statistics are also presented.) The wide variation in site roughness is readily apparent; the Hematite and Athabasca sites meet the MER safety criterion at 5-m baseline but the others to a greater or lesser degree do not. The ranking of sites in terms of roughness shown here is in good qualitative agreement with results from the analysis of a variety of other disparate datasets (see http://marsoweb.nas.nasa.gov/landingsites/mer2003/mer2003.html for reports of the October 2001 and March 2002 MER Landing Site Workshops). As such results are published in greater detail, we plan to compare them with our analysis of the MOC images.

4. Conclusion

The newly developed software and techniques reported here are opening a door to a new realm of Mars topography. The ability to produce DEMs with horizontal resolutions of 10 m and better will be invaluable for selecting future landing sites and will contribute greatly to the study of surface processes. These capabilities will be almost immediately applicable to high-resolution stereoimagery from current and future missions such as 2001 Mars Odyssey, Mars Express and Mars Reconnaissance Orbiter, as well.

5. References

Albertz, J., et al., 1992. The camera experiments HRSC and WAOSS on the Mars 94 mission, *Int. Arch. Photogramm. Remote Sens.*, *29*(B1), 130–137.

Bagnold, F. R. S., 1954. The Physics of Blown Sand and Desert Dunes. Methuen, New York.

Caplinger, M. A., and M. C. Malin, 2001. The Mars Orbiter Camera geodesy campaign. *J. Geophys. Res.*, 106(E10) pp. 23,595–23,606.

Christensen, P., et al., 1999. The Thermal Emission Imaging System (THEMIS) Instrument for the 2001 Orbiter. *Lunar Planet. Sci.,* XXX, Abstract #1470, Lunar and Planetary Institute, Houston (CD-ROM).

Cook, A. C., et al., 1996. Clementine imagery: selenographic coverage for cartographic and scientific use. *Planet. Space Sci*., 44(10), pp. 1135–1148.

Duxbury, T. C., Kirk, R. L., Archinal, B. A., and Neumann, G. A., 2002. Mars Geodesy/Cartography working Group recommendations on Mars cartographic constants and coordinate systems, *Int. Arch. Photogramm. Remote Sens*., submitted (this conference).

Eliason, E., 1997. Production of digital image models using the ISIS system. *Lunar Planet. Sci.,* XXVIII*,* pp. 331–332, Lunar and Planetary Institute, Houston.

Gaddis, L. et al., 1997. An overview of the Integrated Software for Imaging Spectrometers (ISIS). *Lunar Planet. Sci.,* XXVIII*,* pp. 387–388, Lunar and Planetary Institute, Houston.

Greeley, R., Draft, J. D., Kuzmin, R. O., and Bridges, N. T., 2000. Mars Pathfinder landing site: Evidence for a change in wind regime from lander and orbiter data. *J. Geophys. Res.*, 105, pp. 1829–1840.

Herkenhoff, K. E., Bridges, N. T., and Kirk, R. L., 1999. Geologic studies of the Mars Surveyor 1998 landing area. *Lunar Planet. Sci.,* XXX, Abstract #1120, Lunar and Planetary Institute, Houston (CD-ROM).

Herkenhoff, K. E., Soderblom, L. A., and Kirk, R. L., 2002. MOC Photoclinometry of the North Polar Residual Cap. *Lunar Planet Sci*., XXXIII, Abstract #1714, Lunar and Planetary Institute, Houston (CD-ROM).

Howington-Kraus, E., Kirk, R., Galuszka, D., Hare, T., and Redding, B., 2002a. Validation of the USGS sensor model for topographic mapping of Venus using Magellan radar stereoimagery. Lunar Planet. Sci., XXXIII, Abstract #1986, Lunar and Planetary Institute, Houston (CD-ROM).

Howington-Kraus, E., Soderblom, L, Kirk, R., Giese, B., and Oberst, J., 2002b. USGS and DLR topographic mapping of Comet Borrelly. *Int. Arch. Photogramm. Remote Sens*., submitted (this conference).

Howington-Kraus, E., Kirk, R. L., Redding, B., and Soderblom, L. A., 1995. High-resolution topographic map of the Ares-Tiu landing site from Viking Orbiter data. In: Mars Pathfinder Landing Site Workshop II, LPI Tech. Rep. 95-01, pp. 38–39; map reproduced in Tanaka, K. L., 1997. Sedimentary Hhstory and mass flow structures of Chryse and Acidalia Planitia, Mars. *J. Geophys. Res*., 102, pp. 4131–4149.

Ivanov, A. B., and Lorre, J. J., 2002. Analysis of Mars Orbiter Camera Stereo Pairs. *Lunar Planet. Sci.,* XXXIII, Abstract #1845, Lunar and Planetary Institute, Houston (CD-ROM).

Kirk, R. L., 1987. *III. A fast finite-element algorithm for two-dimensional photoclinometry*, Ph.D. Thesis (unpubl.), Caltech. pp. 165–258.

Kirk., R. L., et al.., 1999a. Digital photogrammetric analysis of the IMP camera images: Mapping the Mars Pathfinder landing site in three dimensions. *J. Geophys. Res*., 104(E4), pp. 8869–8887.

Kirk, R. L., Barrett, J., and Howington-Kraus, E., 1999b. A database of Viking Orbiter image coverage for cartographic and scientific use. *Lunar Planet. Sci.,* XXX, Abstract #1857, Lunar and Planetary Institute, Houston (CD-ROM).

Kirk, R. L., Howington-Kraus, E., and Archinal, B., 2001a. High Resolution Digital Elevation Models fo Mars from MOC Narrow Angle Stereoimages. ISPRS-ET Working Group IV/9 Workshop "Planetary Mapping 2001", online at http://wwwflag.wr.usgs.gov/USGSFlag/Space/Isprs/Flagstaff2001/abstracts/Isprs_etm_OCT01_kirk_mars_moc_stereo. pdf.

Kirk, R. L., Howington-Kraus, E., and Archinal, B., 2002. Topographic analysis of candidate Mars Exploration Rover landing sites from MOC Narrow-Angle stereoimages. *Lunar Planet. Sci.,* XXXIII, Abstract #1988, Lunar and Planetary Institute, Houston (CD-ROM).

Kirk, R. L., Howington-Kraus, E., and Rosiek, M., 2000a. Recent planetary topographic mapping at the USGS, Flagstaff: Moon, Mars, Venus, and beyond, *Int. Arch. Photogramm. Remote Sens.,* XXXIII(B4)**,** 476 (CD-ROM).

Kirk, R. L., Thompson, K. T., Becker, T. L., and Lee, E. M., 2000b. Photometric modelling for planetary cartography. *Lunar Planet. Sci*., XXXI, Abstract #2025, Lunar and Planetary Institute, Houston (CD-ROM).

Kirk, R. L., Thompson, K. T., and Lee, E. M., 2001b. Photometry of the martian atmosphere: An improved practical model for cartography and photoclinometry. *Lunar Planet. Sci.,* XXXII, Abstract #1874, Lunar and Planetary Institute, Houston (CD-ROM).

Malin, M. C., et al., 1992. Mars Observer Camera. *J. Geophys. Res.,* 97, pp. 7699–7718.

Malin, M. C., et al., 1998. Early views of the martian surface from the Mars Orbiter Camera of Mars Global Surveyor, *Science,* 279*,* pp. 1681–1685.

Malin, M. C., and Edgett, K. S., 2001. Mars Global Surveyor Mars Orbiter Camera: Interplanetary cruise through primary mission. *J. Geophys. Res.*, 106(E10) pp. 23,429–23,570.

McEwen, A. S., et al., 2002. HiRISE: The High Resolution Imaging Science Experiment for Mars Reconnaissance Orbiter. LPS XXXIII, Abstract #1163, Lunar and Planetary Institute, Houston (CD-ROM).

Miller, S.B. and Walker, A. S., 1993. Further developments of Leica digital photogrammetric systems by Helava. *ACSM/ASPRS Annual Convention and Exposition Technical Papers*, 3, pp. 256–263.

Miller, S.B. and Walker, A.S., 1995. Die Entwicklung der digitalen photogrammetrischen Systeme von Leica und Helava. *Z. Photogramm. Fernerkundung,* 1/95, pp. 4–16.

Neumann, G. A., Rowlands, D. D., Lemoine, F. G., Smith, D. E., and Zuber, M. T., 2001. The crossover analysis of Mars Orbiter Laser Altimeter data. *J. Geophys. Res.*, 106(E10) pp. 23,753–23,768.

Rosiek, M. R., Kirk., R., Hare, T., and Howington-Kraus, E., 2001a. Utilizing Mars Digital Image Model (MDIM) and Mars Orbiter Laser Altimeter (MOLA) data for photogrammetric control. ISPRS-ET Working Group IV/9 Workshop "Planetary Mapping 2001", online at http://wwwflag.wr.usgs.gov/USGSFlag/Space/Isprs/Flagstaff2001/abstracts/isprs_etm_OCT01_rosiek_mars_photogrammetry.pdf.

Rosiek, M. R., Kirk., R., Hare, T., and Howington-Kraus, E., 2001b. Combining lunar photogrammetric topographic data with Clementine LIDAR data. ISPRS-ET Working Group IV/9 Workshop "Planetary Mapping 2001", online at http://wwwflag.wr.usgs.gov/USGSFlag/Space/Isprs/Flagstaff2001/abstracts/isprs_etm_OCT01_rosiek_moon_topography.pdf.

Seidelmann, P. K., et al., 2002. Report of the IAU/IAG working group on cartographic coordinates and rotational elements of the planets and satellites: 2000. *Celest. Mech. Dyn. Astron.,* 82, pp. 83–110.

Smith, D. E., et al., 1999. The global topography of Mars and implications for surface evolution, *Science,* 284, pp. 1495–1503.

Smith, D. E., et al., 2001. Mars Orbiter Laser Altimeter: Experiment summary after the first year of global mapping of Mars. *J. Geophys. Res.*, 106(E10) pp. 23,689–23,722.

Soderblom, L. A., Kirk., R. L., and Herkenhoff, K. E., 2002. Accurate fine-scale topographic profiles in the martian south polar region from MOLA-Calibrated photometric modeling of MOC NA images. Lunar Planet. Sci. XXXIII, Abstract #1254, Lunar and Planetary Institute, Houston (CD-ROM).

Torson, J. and Becker, K., 1997. ISIS: A software architecture for processing planetary images. *Lunar Planet. Sci.,* XXVIII*,* pp. 1443-1444, Lunar and Planetary Institute, Houston.

Turcotte, D. L., 1997. *Fractals and Chaos in Geology and Geophysics*. Cambridge Univ. Press, New York.

Zuber, M. T., et al., 1992. The Mars Observer Laser Altimeter investigation, *J. Geophys. Res.,* 97, pp. 7781–7797.

Table 1. MOC Stereo Image Pairs of Past US Mars Landing Sites

Site	Image	Lon (°)	Lat (°)	Res (m)	ε (°)	ι (°)	Sun Az (°)	VO Res (m)
Viking 1	SP1-23503	48.30	22.59	2.6	31.4	50.5	53.4	16
	SP1-25403	48.30	22.49	2.5	22.3	54.7	43.9	
Mars Pathfinder	SP1-25603	33.50	19.30	3.2	30.7	56.1	38.0	38
	SP1-23703	33.60	19.20	2.6	21.4	50.9	46.6	
Mars Polar Lander	M11-01286	-76.96	200.15	1.4	0.0	55.1	228.3	130
	M11-01563	-76.65	195.55	1.4	1.3	54.9	228.2	
	M11-03519	-76.67	195.69	1.8	29.7	69.5	246.5	

In Tables 1 and 2 Lon, Lat are planetographic/west longitude and latitude, Res is resolution, ε and ι are emission and incidence angles, Sun Az is azimuth of Sun measured clockwise from east, and VO Res is approximate resoluton of best available Viking Orbiter images at given location.

Table 2. MOC Stereo Image Pairs of MER Landing Sites Mapped to Date

Site	Image	Lon (°)	Lat (°)	Res (m)	ε (°)	ι (°)	Sun Az (°)	VO Res (m)
Athabasca Vallis	M07-05928	205.00	7.64	5.85	0.09	44.01	149.7	130
	E10-02604	205.00	8.70	6.18	17.98	42.23	127.4	
	E05-00197	204.00	9.28	6.61	19.21	41.72	174.9	
	M07-00614	204.00	9.66	5.87	0.01	43.28	156.7	
Eos Chasma	E02-02855	41.47	-13.46	4.3	0.2	48.2	224.8	57
	E04-01275	41.50	-13.46	3.3	21.9	47.0	209.6	
	E02-02855	42.00	-13.47	2.87	0.16	44.28	214.0	
	E04-01275	41.90	-13.62	3.00	17.97	23.33	144.5	
Gusev Crater	E02-00665	184.06	-14.96	2.9	0.2	50.7	235.3	76
	E02-01453	184.05	-14.87	3.3	22.1	48.3	234.6	
	E01-00341	184.00	-15.11	2.85	0.07	52.32	238.7	
	E05-00471	184.00	-15.07	2.96	9.99	43.25	209.8	
Isidis Planitia	E02-01301	275.19	4.64	3.1	13.0	37.4	206.9	53
	E02-02016	275.21	4.66	2.9	0.2	38.6	214.1	
Melas Chasma	E02-00270	77.77	-8.87	2.9	0.2	46.8	219.9	68
	E05-01626	77.76	-8.82	3.0	12.8	40.2	196.0	
	M0-04367	77.40	-8.80	2.84	0.21	37.69	161.0	
	E09-02618	77.20	-8.74	3.01	18.09	32.72	137.2	
	M04-00361	77.80	-8.70	2.85	0.20	41.01	192.1	
	E12-00720	77.60	-8.86	3.01	17.94	22.73	137.6	

Table 3. Slope Statistics for candidate MER Landing Sites

Site	Set	Sub Area	DEM from	Baseline (m)	RMS Bidir Slope (°)	RMS Adir Slope (°)	99% Adir Slope (°)	Correction to 5 m Base	99% Adir Slope@ 5 m	P(Adir≥15°) @ 5 m (%)	Remarks
Athabasca	1	a	PC	5.87	1.26	1.72	5.02	1.020	5.12	0.001	NE of ellipse but similar
		b	PC	5.87	0.94	1.48	3.77	1.057	3.97	0.001	"
		c	PC	5.87	1.25	1.86	4.85	1.019	4.99	0.001	"
Athabasca	2	n	ST	10	3.39	4.72	15.67	1.125	17.64	0.019	S of ellipse, higher standing
Athabasca	3	a	ST	20	2.48	3.45	10.20	1.409	11.64	0.004	
		c	PC	5.87	3.99	5.35	13.79	1.007	13.88	0.006	
		d	PC	5.87	2.66	3.48	8.50	1.010	8.58	0.001	
Eos	1	nc	ST	10	6.27	9.22	34.39	1.092	37.56	0.072	
		nd	PC	3	5.82	7.07	23.50	0.927	22.95	0.029	PC area misses hills
Eos	2	a	ST	10	6.05	7.97	25.26	1.189	30.03	0.087	
		c	PC	2.87	8.10	9.61	28.20	1.005	28.33	0.082	
		d	PC	2.87	10.58	13.82	35.40	1.005	35.57	0.239	PC area dominated by hills
Gusev	1	a	ST	10	2.80	4.93	16.29	1.076	17.53	0.015	Smooth interior of small crater
		c	ST	10	5.63	8.20	24.95	1.066	26.61	0.078	Knobby S of small crater
		d	PC	3	4.20	5.23	15.31	0.982	15.03	0.010	Smooth interior of small crater
		e	PC	3	9.35	11.67	22.30	0.990	31.97	0.163	Knobby S of small crater
Gusev	2	a	ST	10	8.32	11.37	37.58	1.048	37.38	0.157	Gusev 2 areas similar to 1c/e
		b	ST	10	12.75	16.52	48.17	1.049	50.52	0.340	
		c	PC	3	9.00	11.65	30.80	0.989	30.45	0.166	
		d	PC	3	12.23	15.92	42.99	0.985	52.36	0.299	
Hematite	2	a	PC	2.9	4.89	9.45	24.38	0.791	19.29	0.037	Albedo variations, not slopes
		b	PC	2.9	1.25	1.82	4.94	0.946	4.68	0.001	Bland area, typical
		c	PC	2.9	2.21	3.38	9.46	0.933	8.83	0.001	Exposed rougher area
Isidis	1	nb	ST	10	4.66	6.39	25.60	1.202	30.78	0.037	
		nc	PC	3	5.70	7.45	22.32	0.983	21.93	0.027	
		sa	ST	10	4.12	5.80	20.08	1.058	21.24	0.027	
		sb	PC	3	8.49	10.78	31.18	0.987	30.78	0.121	
Melas	1	a	ST	10	2.72	4.86	14.34	1.000	14.34	0.008	Does not resolve dunes
		b	ST	10	1.56	2.66	7.74	1.000	7.74	0.001	"
		c	ST	10	2.43	4.11	12.61	1.000	12.61	0.004	"
		e	PC	3	13.19	15.85	41.37	0.923	38.17	0.289	Dunes resolved!
Melas	2	a	ST	10	9.96	12.89	43.42	1.187	51.52	0.233	Layers
Melas	3	a	ST	10	11.37	14.37	53.80	1.273	68.49	0.274	"

Set refers to MOC stereopair within a given landing site, in the order listed in Table 2, except that sets Athabasca 1 and Hematite 2 are single images used for photoclinometry. Subarea refers to different regions within each DEM selected for slope analysis. PC = photocliometry, ST = stereo. Bdir = bidirectional slope, Adir = adirectional slope (gradient). Remarks indicate reasons for assessing some results (subdued) as not representative of the landing site. Adirectional slopes scaled to 5-m baseline also appear in Fig. 8, where non-representative values are plotted with open symbols.